JACS
JOURNAL OF THE AMERICAN CHEMICAL SOCIETY
Communication
pubs.acs.org/JACS

An Advanced Ni–Fe Layered Double Hydroxide Electrocatalyst for Water Oxidation

Ming Gong,[‡,†] Yanguang Li,[‡,†] Hailiang Wang,[‡] Yongye Liang,[‡] Justin Z. Wu,[‡] Jigang Zhou,[§] Jian Wang,[§] Tom Regier,[§] Fei Wei,[⊥] and Hongjie Dai*[,‡]

[‡]Department of Chemistry, Stanford University, Stanford, California 94305, United States
[§]Canadian Light Source Inc., Saskatoon, Saskatchewan S7N 0X4, Canada
[⊥]Department of Chemical Engineering, Tsinghua University, Beijing 100084, China

Supporting Information

ABSTRACT: Highly active, durable, and cost-effective electrocatalysts for water oxidation to evolve oxygen gas hold a key to a range of renewable energy solutions, including water-splitting and rechargeable metal–air batteries. Here, we report the synthesis of ultrathin nickel–iron layered double hydroxide (NiFe-LDH) nanoplates on mildly oxidized multiwalled carbon nanotubes (CNTs). Incorporation of Fe into the nickel hydroxide induced the formation of NiFe-LDH. The crystalline NiFe-LDH phase in nanoplate form is found to be highly active for oxygen evolution reaction in alkaline solutions. For NiFe-LDH grown on a network of CNTs, the resulting NiFe-LDH/CNT complex exhibits higher electrocatalytic activity and stability for oxygen evolution than commercial precious metal Ir catalysts.

Oxygen electrochemistry has been intensely researched in the pursuit of sustainable and efficient energy conversion and storage solutions. Oxygen evolution reaction (OER) is the process of generating molecular oxygen through electrochemical oxidation of water, and it holds a key to a number of important energy conversion and storage processes, such as water-splitting and rechargeable metal–air batteries.[1−7] OER proceeds through multistep proton-coupled electron transfer, and is kinetically sluggish.[8,9] An effective electrocatalyst is needed in order to expedite the reaction, reduce the overpotential, and thus enhance the energy conversion efficiency. Currently, the most active OER catalysts are IrO_2 or RuO_2 in acidic or alkaline solutions,[4,10] but these catalysts suffer from the scarcity and high cost of precious metals. Extensive efforts have been taken to develop highly active, durable, and low-cost alternatives such as first-row transition metal oxides[11−15] and perovskites.[16,17] However, most non-precious metal catalysts developed still underperform the Ir benchmark.

Here, we report a nickel–iron layered double hydroxide (NiFe-LDH)–carbon nanotube (CNT) complex with higher OER catalytic activity and stability than commercial Ir-based catalysts. The key aspects of this catalyst are the formation of ultrathin nanoplates of a highly OER-active NiF-LDH structure [the same structure as alpha-phase nickel hydroxide (α-phase $Ni(OH)_2$] and association of the nanoplates with CNTs that can form interconnected electrically conducting networks. Even though electrodeposited NiFe mixed oxide/hydroxide has been made for OER previously,[18−21] this was the first time that crystalline NiFe-LDH was synthesized chemically to obtain highly active electrocatalysts for OER in alkaline media. The turnover frequency (TOF) of the NiFe-LDH/CNT catalyst exceeded those of any previous Ni–Fe compounds[18,22−25] and was comparable to that of the most active perovskite-based catalyst.[17]

A three-step process was developed to synthesize the NiFe-LDH/CNT complex. Nickel acetate and iron nitrate (with a molar ratio of Ni/Fe = 5) were hydrolyzed and selectively coated onto mildly oxidized multiwalled (MW) CNTs (by a modified Hummers's method with one-third amount of $KMnO_4$; see Supporting Information (SI) for details) in a *N*,*N*-dimethylformamide (DMF) solution at 85 °C. The intermediate product was redispersed in a DMF/H_2O mixed solvent and then subjected to a solvothermal treatment at 120 °C for 12 h, followed by a second solvothermal step at 160 °C for 2 h. The solvothermal treatment led to the crystallization of nanoplates and partial reduction of the oxidized CNTs.

The size, morphology, and structure of the resulting material were characterized by scanning electron microscopy (SEM) and transmission electron microscopy (TEM). SEM (Figure 1a) showed that ultrathin plates (reflected by poor image contrast) were grown over a CNT network. TEM (Figure 1b) showed that the nanoplate size was typically ∼50 nm and nearly transparent to electron beams due to the ultrathin nature. We also observed 3–5 nm nanoparticles with higher contrast along the edges of nanoplates and the outer walls of CNTs. High-resolution TEM (Figure 1c) of these nanoparticles revealed a different set of lattice fringes corresponding to iron oxide (FeO_x). Spatially resolved energy dispersive spectroscopy (EDS) analysis (spatial resolution of ∼2 nm) also suggested a small amount of FeO_x nanoparticles distributed over the nanoplate/CNT complex (Figure S1).

The X-ray diffraction (XRD) pattern (Figure 1d) of the final product was consistent with the α-phase $Ni(OH)_2$ (the same as LDH) with a greater interlayer distance compared to β-phase $Ni(OH)_2$. From the widths of (003) and (006) diffraction peaks, the thickness of nanoplates was estimated to be ∼5 nm,

Received: March 19, 2013
Published: May 23, 2013

   dx.doi.org/10.1021/ja4027715 | *J. Am. Chem. Soc.* 2013, 135, 8452–8455

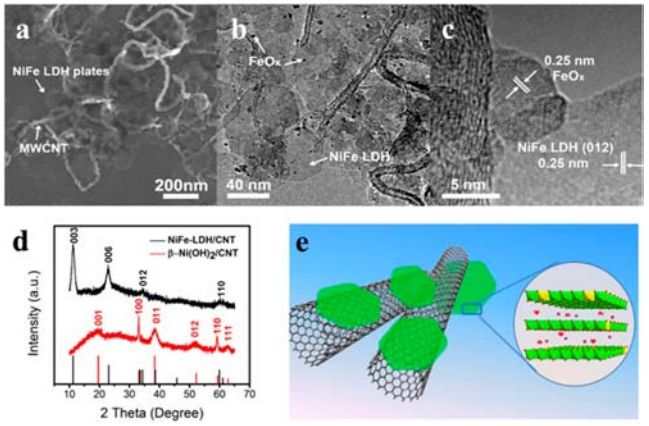

Figure 1. Ultrathin nickel−iron layered double hydroxide nanoplates grown on carbon nanotubes. (a) SEM image of NiFe-LDH nanoplates grown over a network of mildly oxidized MWCNTs. (b,c) TEM images of the NiFe-LDH/CNT hybrid. Arrows point to individual NiFe-LDH plates and smaller iron oxide particles. (d) XRD spectra of NiFe-LDH/CNT (black) and a control β-Ni(OH)$_2$/CNT sample (red, synthesized without the iron precursor). The lines correspond to standard XRD patterns of α-Ni(OH)$_2$ (black, JCPDS card No. 38-0715) and β-Ni(OH)$_2$ (red, JCPDS card No. 14-0117). (e) Schematic showing the hybrid architecture and LDH crystal structure.

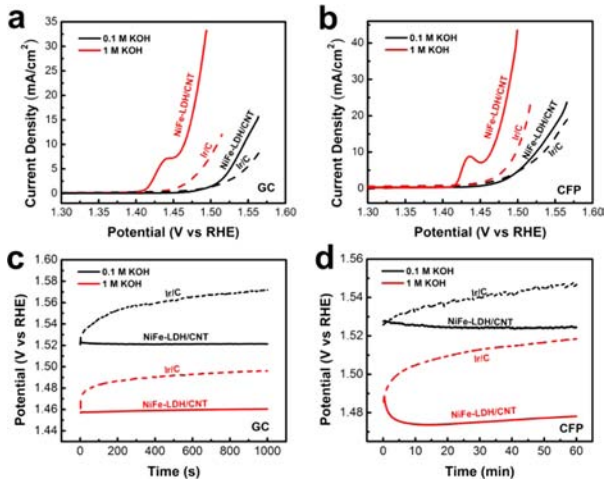

Figure 2. Electrochemical performance of NiFe-LDH/CNT hybrid OER catalyst. (a) *iR*-corrected polarization curves of NiFe-LDH/CNT hybrid and Ir/C catalyst on GC electrode in 0.1 and 1 M KOH, measured with a catalyst loading of 0.2 mg/cm^2 for both NiFe-LDH/CNT and Ir/C at a continuous electrode rotating speed of 1600 rpm. (b) *iR*-corrected polarization curves of NiFe-LDH/CNT hybrid and Ir/C catalysts on carbon fiber paper, measured with a catalyst loading of 0.25 mg/cm^2. See SI and Figure S5 for details of *iR* correction. (c) Chronopotentiometry curves of NiFe-LDH/CNT hybrid and Ir/C catalyst on GC electrode at a constant current density of 2.5 mA/cm^2. (d) Chronopotentiometry curves of NiFe-LDH/CNT hybrid and Ir/C catalyst on CFP at a constant current density of 5 mA/cm^2.

confirmed by atomic force microscopy topological height analysis (Figure S2). Interestingly, pure β-phase Ni(OH)$_2$ nanoplates on CNT networks were synthesized by the same method in the absence of any iron precursors. The drastically different phases suggested that incorporation of an Fe precursor to Ni induced the formation of NiFe hydroxide in LDH structure. It was known that Fe^{3+} could replace Ni^{2+} in the Ni(OH)$_2$ lattice, forming a stable LDH structure.[26−30] The excessive cationic charge due to Fe^{3+} was balanced by anion intercalation between the hydroxide layers.[28] X-ray photoelectron spectroscopy (Figure S3) corroborated the existence of both Fe and Ni in the hybrid material. The Fe species was found to be mostly in the +3 oxidation state from the high-resolution Fe 2p spectrum (Figure S3d). X-ray absorption near-edge structure (XANES) measurements confirmed the Ni^{2+} and Fe^{3+} oxidation states (Figure S4a,b). Both Fe and Ni signals were detected on nanoplates in areas free of decorating FeO$_x$ nanoparticles by spatially resolved EDS (Figure S1). These results suggested the synthesis of ultrathin NiFe-LDH nanoplates decorated with FeO$_x$ nanoparticles grown over a network of gently oxidized MWCNTs (Figure 1).

We investigated the electrocatalytic OER activity of NiFe-LDH/CNT in alkaline solutions (0.1 and 1 M KOH) in a standard three-electrode system (see details in SI). The material was uniformly cast onto a glassy carbon (GC) electrode (loading ∼0.2 mg/cm^2) for recording *iR*-corrected OER polarization curves at a slow scan rate of 5 mV/s to minimize capacitive current (Figure S5). During the measurements, the working electrode was continuously rotating at 1600 rpm to remove the generated oxygen bubbles. For comparison, a commercial Ir/C catalyst (20 wt% Ir on Vulcan carbon black from Premetek Co. with the same ∼0.2 mg/cm^2 loading) was measured side-by-side. In 0.1 M KOH, the anodic current recorded with the NiFe-LDH/CNT catalyst showed a sharp onset of OER current at ∼1.50 V versus the reversible hydrogen electrode (RHE) (Figure 2a). The Ir/C catalyst afforded a similar onset potential, but its OER current density fell below that of our NiFe-LDH/CNT hybrid at ∼1.52 V. In 1 M KOH, the OER onset potential of the NiFe-LDH/CNT reduced considerably to ∼1.45 V vs RHE (Figure 2a). We also loaded and tested the catalysts on carbon fiber paper (CFP, loading density ∼0.25 mg/cm^2, effective area 1 cm^2) and observed an activity trend and pH dependence (Figure 2b) similar to those on a rotating disk electrode. The peak around 1.43 V of NiFe-LDH/CNT in 1 M KOH is assigned to the Ni(II)/Ni(III or IV) redox process.[31] The NiFe-LDH/CNT electrocatalyst was among the most active non-precious metal electrocatalysts[11−15,24,32] (Table S1).

We calculated a high TOF of 0.56 s^{-1} associated with NiFe-LDH/CNT at an overpotential of 300 mV in 1 M KOH, assuming all the metal sites were involved in the electrochemical reaction (see SI). This value represented the lower limit, since some of these metal sites in the nanoplates were electrochemically nonaccessible. Even in this case, the TOF of our NiFe-LDH/CNT catalyst was still about 3 times higher than those previous reported for mixed nickel and iron oxide electrocatalysts (the previous highest TOF was 0.21 s^{-1} at similar experimental conditions).[18,22−25] Our result here also compared favorably to the TOF of a high-performance perovskite material (∼0.6 s^{-1} calculated based on only surface-active sites).[17]

Besides high OER activity, the NiFe-LDH/CNT catalyst exhibited good durability in alkaline solutions (Figure 2c,d). When biased galvanostatically at 5 mA/cm^2 on CFP electrodes, the NiFe-LDH/CNT catalyst had a nearly constant operating potential, at ∼1.52 V (corresponding to an overpotential of 0.29 V) in 0.1 M KOH, whereas the Ir/C catalyst showed an increase in overpotential by ∼20 mV (Figure 2d). In 1 M KOH (Figure 2d), the working potential of NiFe-LDH/CNT was lowered to ∼1.48 V to deliver a 5 mA/cm^2 current density, and the catalyst was also more stable than the commercial Ir

dx.doi.org/10.1021/ja4027715 | J. Am. Chem. Soc. 2013, 135, 8452−8455

catalyst. Consistent OER durability data were also recorded on rotating disk electrodes (Figure 2c).

We fitted the polarization curves obtained with the NiFe-LDH/CNT hybrid on CFP electrodes at various pH's to the Tafel equation $\eta = b \log(j/j_0)$, where η is the overpotential, b is the Tafel slope, j is the current density, and j_0 is the exchange current density.[33] The NiFe-LDH/CNT catalyst exhibited a Tafel slope of $b \approx 35$ mV/decade in 0.1 M KOH and $b \approx 31$ mV/decade in 1 M KOH (Figure 3a). This value was smaller

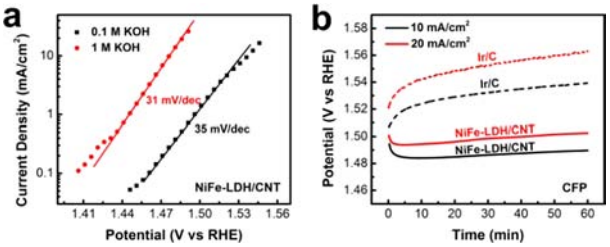

Figure 3. (a) Tafel plots of NiFe-LDH/CNT catalyst loaded on CFP (at 0.25 mg/cm^2) recorded at 0.1 mV/s in 0.1 and 1 M KOH. (b) Chronopotentiometry curves of NiFe-LDH/CNT hybrid and Ir/C catalyst loaded on CFP (at 0.25 mg/cm^2) under higher current densities of 10 and 20 mA/cm^2.

than that of Ir/C reference (~40 mV/decade).[33] Consistently, the NiFe-LDH/CNT catalyst exhibited higher activity and stability than Ir/C at current densities of 10 and 20 mA/cm^2 (~50 and ~60 mV difference in overpotential after 1 h operation, Figure 3b). Similar trends of OER activity and stability were observed under maximal loading of the hybrid catalysts on CFP (Figure S6).

To confirm oxygen evolution, we carried out high-current and long-time electrolysis by passing through more charges than would be needed for completely oxidizing carbon in the NiFe-LDH/CNT catalysts (Figure S7). High OER activities remained, and CNT structures were observed in the catalyst after the long OER operation when examined by SEM and TEM (Figure S7c,d), suggesting that the CNTs in the catalyst complex were not removed by oxidative etching under the OER conditions used. Note that pure CNTs without NiFe-LDH showed negligible current in the <1.5 V voltage range (Figure S8, green curve) over which OER was highly active for the NiFe-LDH/CNT catalyst (Figure S8, black curve). Clearly, the high anodic current density observed with the NiFe-LDH/CNT catalyst was dominant for OER catalyzed by the hybrid material rather than oxidative corrosion of CNTs. We analyzed the gaseous products from the OER of NiFe-LDH/CNT catalysts on non-carbon-based electrode using gas chromatography and found that oxygen was the only product, with a Faradaic efficiency similar to that of an IrO_2 benchmark (IrO_2 nanoparticle from Premetek Co.) (Figure S9).

Our electrochemical data suggested that the NiFe-LDH/CNT complex was a novel electrocatalyst material with high OER activity and stability in basic solutions. The high electrocatalytic performance was mainly attributed to the NiFe-LDH phase. Strong association of the LDH with CNTs further facilitated charge transport and improved the catalyst (Figure 4b). In a series of control experiments, we observed that the NiFe LDH material alone without CNTs showed high activity for OER catalysis and was superior to amorphous NiFe oxide formed by electrodeposition[18] on GC electrodes (Figure 4a). The NiFe-LDH phase was also more active for OER than a

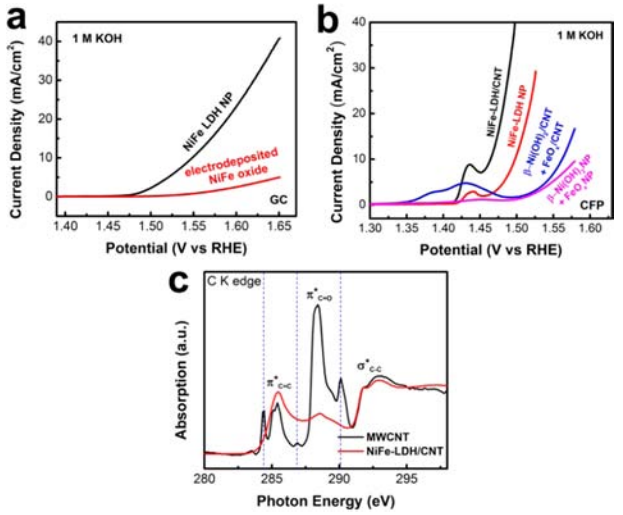

Figure 4. (a) Polarization curves of free NiFe LDH nanoplates (loading of 0.2 mg/cm^2) without any CNTs and electrodeposited NiFe oxide [cathodically electrodeposited under the current density of 1 mA/cm^2 for 600 s, 0.09 M $Ni(NO_3)_2$ and 0.01 M $Fe(NO_3)_3$ solution (pH 2) (loading of 2.4 mg/cm^2)[18]] in 1 M KOH on GC electrodes. (b) Polarization curves of NiFe-LDH/CNT hybrid, NiFe-LDH plate alone, a physical mixture of β-$Ni(OH)_2$/CNT and FeO_x/CNT, and a physical mixture of β-$Ni(OH)_2$ and FeO_x nanoparticles loaded on CFP (with a loading of 0.25 mg/cm^2) in 1 M KOH. (c) C K-edge XANES spectra of NiFe-LDH/CNT (black) and pure MWCNT (red) without coupling to LDH. The blue dashed lines mark defects at 284.4 eV, $\sigma^*_{C\text{-}H}$ at 286.9 eV, and $\pi^*_{O\text{-}C(O)\text{-}O}$ (carbonate) at 290.1 eV.

mixture of β-$Ni(OH)_2$ and FeO_x nanoparticles, with and without association with CNTs (Figure 4b). When loaded into Ni foams to facilitate better contact and charge transport by the Ni foam substrate, the NiFe-LDH nanoplates alone without any carbon additive exhibited high activity and stability over several days of OER operation at 20 mA/cm^2 in 1 M KOH (Figure S10). We also performed XRD analysis of the NiFe-LDH/CNT catalysts after OER operation for 3 h. The XRD pattern was consistent with a crystalline NiFe-LDH phase (Figure S7e), suggesting no change in the LDH phase through OER catalysis. Thus, we chemically synthesized a crystalline NiFe-LDH phase as a highly OER-active material in basic solutions.

Interaction between NiFe-LDH and CNTs afforded by direct nucleation and growth of LDH nanoplates on the functional groups on CNTs contributed to the optimal OER activity of the NiFe-LDH/CNT complexes. XANES measurements were employed to reveal the interactions (Figure 4c). At carbon K-edge absorption, the NiFe-LDH/CNT showed a drastic increase of carbonyl π^* peak intensity at ~288.5 eV[34] compared to the CNT control without any NiFe-LDH plates. This was attributed to the formation of M−O−C (M = Ni, Fe) bonding via the carboxyl group, leading to large perturbations to the carbon atoms in the carbonyl groups. The drastic changes in the X-ray spectroscopy revealed strong interaction effects of NiFe-LDH nanoplates and CNTs, which facilitated charge transport and favored high OER activity and stability. Accordingly, NiFe-LDH/CNT hybrid material exhibited higher OER activity than NiFe-LDH nanoplate alone, NiFe-LDH mixed with carbon black, and NiFe-LDH mixed with CNT (Figures 4b and S11).

In conclusion, we devised a strategy for the nucleation and growth of NiFe-LDH nanoplates on mildly oxidized CNTs. We uncovered the high intrinsic OER electrocatalytic activity of the

dx.doi.org/10.1021/ja4027715 | J. Am. Chem. Soc. 2013, 135, 8452−8455

crystalline NiFe-LDH phase and observed the underlying CNT network enhancing electron transport and facilitating high OER activity of the NiFe-LDH nanoplate/CNT complex. This led to an electrocatalyst that outperformed Ir in both activity and stability in basic solutions, opening a new venue to advanced, low-cost oxygen evolution electrocatalysts for energy applications such as high performance Zn-air batteries.[35]

■ ASSOCIATED CONTENT

Supporting Information

Experimental procedures and supporting data. This material is available free of charge via the Internet at http://pubs.acs.org.

■ AUTHOR INFORMATION

Corresponding Author

hdai@stanford.edu

Author Contributions

†M.G. and Y.L. contributed equally.

Notes

The authors declare no competing financial interest.

■ ACKNOWLEDGMENTS

This work was supported partially by Intel and a Stinehart/Reed Award from the Stanford Precourt Institute for Energy. We thank Prof. M. Kanan's group for use of GC equipment.

■ REFERENCES

(1) Gray, H. B. *Nat. Chem.* **2009**, *1*, 112.
(2) Kudo, A.; Miseki, Y. *Chem. Soc. Rev.* **2009**, *38*, 253.
(3) Lu, Y. C.; Xu, Z. C.; Gasteiger, H. A.; Chen, S.; Hamad-Schifferli, K.; Shao-Horn, Y. *J. Am. Chem. Soc.* **2010**, *132*, 12170.
(4) Walter, M. G.; Warren, E. L.; McKone, J. R.; Boettcher, S. W.; Mi, Q.; Santori, E. A.; Lewis, N. S. *Chem. Rev.* **2010**, *110*, 6446.
(5) Cheng, F. Y.; Chen, J. *Chem. Soc. Rev.* **2012**, *41*, 2172.
(6) Liang, Y. Y.; Li, Y. G.; Wang, H. L.; Dai, H. J. *J. Am. Chem. Soc.* **2013**, *135*, 2013.
(7) Wang, H.; Dai, H. *Chem. Soc. Rev.* **2013**, *42*, 3088.
(8) Koper, M. T. M. *J. Electroanal. Chem.* **2011**, *660*, 254.
(9) Kanan, M. W.; Nocera, D. G. *Science* **2008**, *321*, 1072.
(10) Lee, Y.; Suntivich, J.; May, K. J.; Perry, E. E.; Shao-Horn, Y. *J. Phys. Chem. Lett.* **2012**, *3*, 399.
(11) Esswein, A. J.; McMurdo, M. J.; Ross, P. N.; Bell, A. T.; Tilley, T. D. *J. Phys. Chem. C* **2009**, *113*, 15068.
(12) Li, Y. G.; Hasin, P.; Wu, Y. Y. *Adv. Mater.* **2010**, *22*, 1926.
(13) Liang, Y. Y.; Li, Y. G.; Wang, H. L.; Zhou, J. G.; Wang, J.; Regier, T.; Dai, H. J. *Nat. Mater.* **2011**, *10*, 780.
(14) Gorlin, Y.; Jaramillo, T. F. *J. Am. Chem. Soc.* **2010**, *132*, 13612.
(15) Cui, B.; Lin, H.; Li, J. B.; Li, X.; Yang, J.; Tao, J. *Adv. Funct. Mater.* **2008**, *18*, 1440.
(16) Bockris, J. O.; Otagawa, T. *J. Electrochem. Soc.* **1984**, *131*, 290.
(17) Suntivich, J.; May, K. J.; Gasteiger, H. A.; Goodenough, J. B.; Shao-Horn, Y. *Science* **2011**, *334*, 1383.
(18) Corrigan, D. A. *J. Electrochem. Soc.* **1987**, *134*, 377.
(19) Indira, L.; Dixit, M.; Kamata, P. V. *J. Power Sources* **1994**, *52*, 93.
(20) Mlynarek, G.; Paszkiewicz, M.; Radniecka, A. *J. Appl. Electrochem.* **1984**, *14*, 145.
(21) Miller, E. L.; Rocheleau, R. E. *J. Electrochem. Soc.* **1997**, *144*, 3072.
(22) Corrigan, D. A.; Bendert, R. M. *J. Electrochem. Soc.* **1989**, *136*, 723.
(23) Merrill, M. D.; Dougherty, R. C. *J. Phys. Chem. C* **2008**, *112*, 3655.
(24) Li, X. H.; Walsh, F. C.; Pletcher, D. *Phys. Chem. Chem. Phys.* **2011**, *13*, 1162.
(25) Trotochaud, L.; Ranney, J. K.; Williams, K. N.; Boettcher, S. W. *J. Am. Chem. Soc.* **2012**, *134*, 17253.
(26) Taibi, M.; Ammar, S.; Schoenstein, F.; Jouini, N.; Fievet, F.; Chauveau, T.; Greneche, J. M. *J. Phys. Chem. Solids* **2008**, *69*, 1052.
(27) Zhao, X. F.; Xu, S. L.; Wang, L. Y.; Duan, X.; Zhang, F. Z. *Nano Res.* **2010**, *3*, 200.
(28) Kahn, A. I.; O'Hare, D. *J. Mater. Chem.* **2002**, *12*, 3191.
(29) Axmann, P.; Glemser, O. *J. Alloys Compd.* **1997**, *246*, 232.
(30) Chou, S. L.; Cheng, F. Y.; Chen, J. *Eur. J. Inorg. Chem.* **2005**, *2005*, 4035.
(31) Corrigan, D. A.; Knight, S. L. *J. Electrochem. Soc.* **1989**, *136*, 613.
(32) Kleiman-Shwarsctein, A.; Hu, Y. S.; Stucky, G. D.; McFarland, E. W. *Electrochem. Commun.* **2009**, *11*, 1150.
(33) Trasatti, S. *Electrodes of Conductive Metallic Oxides*; Elsevier: New York, 1981.
(34) Kuznetsova, A.; Popova, I.; Yates, J. T., Jr.; Bronikowski, M. J.; Huffman, C. B.; Liu, J.; Smalley, R. E.; Hwu, H. H.; Chen, J. G. *J. Am. Chem. Soc.* **2001**, *123*, 10699.
(35) Li, Y. G.; Gong, M.; Liang, Y. Y.; Feng, J.; Kim, J. E.; Wang, H. L.; Hong, G. S.; Zhang, B.; Dai, H. J. *Nat. Comm.* **2013**, *4*, 1805.